Wavelength-dependence of the photothermal efficiency of gold nanoparticles in solution by Z-scan photothermal lens spectroscopy

Julien-Bilal Zinoune, Christophe Cassagne, Martinus H.V. Werts, Matthieu Loumaigne, Mihaela Chis, Georges Boudebs

Wavelength-dependence of the photothermal efficiency of gold nanoparticles in solution by Z-scan photothermal lens spectroscopy

Julien-Bilal Zinoune [1, 4], Christophe Cassagne [1], Martinus H. V. Werts [2], Matthieu Loumaigne [3], Mihaela Chis [1, 4], Georges Boudebs [1,*]

[1] ***Univ Angers***, ***LPHIA***, *SFR MATRIX, F-49000 Angers, France*

[2] ***Univ Rennes***, *CNRS, SATIE – UMR8029, F-35000 Rennes, France*

[3] ***Univ Angers***, ***MOLTECH-ANJOU***, *SFR MATRIX, F-49000 Angers, France*

[4] ***ESAIP***, ***CERADE***, *18, rue du 8 mai 1945, 49180 St-Barthélemy d'Anjou Cedex, France*

* Corresponding author: Tel: (33) 2.41.73.54.26, Fax: (33) 2.41.73.52.16,
e-mail: georges.boudebs@univ-angers.fr

ACCEPTED MANUSCRIPT – AUTHOR'S VERSION

Final published version can be found at: https://doi.org/10.1016/j.cplett.2023.140501

Citation: J.-B. Zinoune et al., *Chem. Phys. Lett.* **2023**, *823,* 140501

ABSTRACT

Using continuous-wave (cw) single-beam Z-scan technique, the absorption and scattering efficiencies of spherical gold nanoparticles (NPs) of varying diameter are determined experimentally through the thermal lens (TL) effect for three different wavelengths in the blue, the green and the red. The main characteristics of the measurement method are detailed, extending the usual experimental procedure for weak absorption with Gaussian beams to higher absorption with top-hat beams. To confirm the validity of our approach, the experimental TL data were compared to the theoretical values from Mie theory and found to be in good agreement within the experimental errors. As expected, the photothermal efficiency of spherical gold NPs increases with lower diameters and towards shorter wavelengths.

Keywords: Thermal lens, Z-scan, linear absorption, scattering efficiency, Mie theory, gold nanoparticles.

1. INTRODUCTION

In terms of optical properties, nanoparticles (NPs) are characterized by their ability to scatter and absorb light. Nanoparticles made of gold, silver or other conducting materials often exhibit particularly strong absorption and scattering of light over specific spectral bands owing to their localized surface plasmons resonances.[1, 2] The light absorbed is swiftly and nearly quantitatively converted into heat, resulting in bulk photothermal heating of the surrounding medium.[3] This photothermal effect may be used in a variety of applications such as biological microscopy,[4] cancer treatment,[5] or solar energy conversion.[6] Light scattering from plasmonic NPs can be sufficiently strong to enable single-particle observations in dark-field microscopy[7] and is of interest for sensing and in vitro diagnostics.[8]

Properties such as the optical resonance wavelength, the extinction cross-sections and the relative contributions of light scattering and light absorption are of paramount importance in the characterization of nanoparticles and their selection and optimization for a specific application. On one hand, quantitative information on these properties may be obtained from theoretical calculations, for example using Mie theory,[2] or from numerical calculations of the scattering, extinction and absorption of NPs of different shapes.[1] On the other hand, quantitative experimental approaches are essential for the characterization of NPs, for verifying theoretical predictions, and ensuring the quality of the NP sample. Another metrological problem would be to determine the exact light intensity that induces a physical phenomenon inside the tested sample. This is the case with solutions where the compounds are not completely dissolved or bulk specimen presenting nanoclusters or aggregates scattering the incident light therefore misleading the measurements of the required coefficients: for example, when measuring the third order optical nonlinearity in different media.[9, 10, 11, 12]

If the extremely weak luminescence of gold NP is neglected,[13] light interacting with a solution of plasmonic NPs is either scattered or converted into heat, quantitative spectroscopic methods based on either one of these phenomena are of particular interest for the characterization of NPs in solution, in addition to standard extinction ("UV-vis") spectroscopy. Quantitative measurements of the light scattering of gold nanospheres in solution have been made by resonant light scattering (RLS) spectroscopy using ideal Rayleigh scatterers (Ludox, ZnO) as references.[2, 14] There is very good agreement between these measurements and the results from Mie theory, and the technique has been applied also to non-spherical particles[15] and multiparticle assemblies.[16, 17] Photothermal measurements provide a complementary view by measuring the fraction of luminous energy not scattered, and give a global balance of the contributions of absorption and scattering. Quantitative measurement of light scattering can become complicated when angle and polarization dependence should be considered,[2, 14] and photothermal measurements may complete and validate the overall scattering versus absorption balance.

The photothermal heating by NPs in solution under laser illumination has been measured using thermocouples in contact with the NP solution.[18, 19] Similar measurements have also been done on molecular dyes.[20] However, the sensitivity of these methods is limited, high laser illumination powers are needed, the response time is long, and quantitative determination of the fraction of light absorbed in the overall extinction is delicate.

Photothermal lens spectroscopy,[21, 22, 23] commonly referred to as thermal lens (TL) spectroscopy (TLS), provides a sensitive and quantitative measurement of photothermal conversion in nanoparticle, molecular and other light-absorbing systems with minimal perturbation of the sample. Indeed, the excitation powers are modest (milliwatts), the induced temperature rise very small (well below 1 K) and the response is fast (sub-second). In addition

to the photothermal conversion efficiency, TLS also gives quantitative access to the thermal diffusivity of the medium.

Whereas TLS has been extensively and successfully applied to molecular systems in solution over the years,[23, 24, 25] studies of NP solutions have only recently emerged. An early application[23, 26] of TLS to gold NP solutions only measured the effect gold nanoparticles on the thermal diffusivity of the NP solution (the 'nanofluid'), but did not consider the photothermal efficiency of the NPs. The measurement of the thermal diffusivity of NP solutions using TL has been extended to differently sized gold NPs[27] and to nanofluids based on other nanomaterials such as carbon nanotubes.[28]

A first TL spectrum of 50 nm spherical gold nanoparticles in aqueous solution was published,[29] although the reported absence of light scattering and near-unity photothermal yield disagree with predictions from Mie theory and measurements by RLS spectroscopy.[2] Subsequent studies on silver NPs found agreement between TLS and predictions from Mie theory concerning the photothermal conversion efficiency.[30, 31] Quantitative single-wavelength TL measurements at 532 nm of 50 nm gold NPs in water were reported by Pedrosa et al. who also evaluated the (very small) temperature rise due to photothermal heating in the experiment.[32] Following the same approach as the work conducted in [33], we used a newly developed Z-scan[34] TL set-up at 532 nm to quantify the absorption and scattering contributions to the light extinction by 5 nm and 50 nm gold nanoparticles in water.[35]

In this paper, we present a multi-wavelength Z-scan TL spectroscopic study of spherical gold nanoparticles in aqueous solution. The experimental set-up and protocol from our previous work[35] have been further improved by using a top-hat beam much more convenient to adapt experimentally to each wavelength by changing the diameter of the circular aperture. The measurements yield the photothermal efficiency, i.e. the fraction of interacting light power that is converted into heat. Since gold NPs convert all absorbed light into heat, this photothermal

efficiency is equal to the ratio of the absorption and extinction cross section. The complement is the light-scattering efficiency, the ratio of the scattering and extinction cross sections. We demonstrate the complementarity of photothermal TLS measurements and quantitative light scattering RLS spectroscopy. The experimental data are compared to theoretical spectra obtained using Mie theory and show a marked wavelength dependence of the photothermal and scattering efficiencies.

2. THEORY

The following symbols will be used: α_a and α_e, absorption and extinction coefficients in m^{-1}, respectively; ρ density in Kg/m^3; I beam intensity in W/m^2; L thickness of the medium (cell) in m; P beam power in W (taking into account the Fresnel reflection); c specific heat in $J/Kg/K$; ω beam radius in m; ΔT temperature variation in$°K$; k thermal conductivity in $J/s/m/K$; λ wavelength in m. The usual TL approximations are assumed following references [35, 36]: i) thin sample; ii) beam-waist considered small when compared to the dimensions of the cell. An expression of the temperature change as a function of radius and time $\Delta T(r,t)$ can be obtained by solving the non-steady state heat equation with a Gaussian beam illuminating the medium:

$$c\rho\frac{\partial}{\partial t}[\Delta T(r,t)] = \dot{q}(r) + k\nabla^2[\Delta T(r,t)]. \qquad (1)$$

The term $\dot{q}$ representing the heat source into a unit volume per unit time at a distance r was approximated in [36], considering a small absorption: $\dot{q}(r) = I_0(r)\alpha_a$ where $I_0(r)$ is the beam intensity entering the sample placed at a position z. The z-dependency will not be considered in this section but will be taken into account later (section 3a.) where it is necessary. As shown in the appendix, the relative error while measuring the scattering efficiency of very absorbing suspensions decreases with the total extinction of the solution. Thus, it is interesting to also consider the case of a solution with moderately high extinction. To achieve this, it is necessary

to adapt the expression for $\dot{q}(r)$ to fit the calculation method to a higher extinction coefficient. The modifications made are presented hereafter.

According to the Beer-Lambert-Bouguer law relating the optical attenuation in the solution to the path length L, the intensity change in the laser light as it passes the absorbing medium $\Delta I(r)$ is expressed by:

$$\Delta I(r) = I_0(r)(1 - e^{-\alpha_a L}). \quad (2)$$

Note that in the special case where $\alpha_a L \ll 1$, we come back to the approximation used in [36] ($\Delta I(r) = I_0(r)\alpha_a L$) but for the more general case with relatively larger absorbance (while remaining with $\alpha_a L < 1$), $\frac{dq}{dt}$ the heat flow then becomes:

$$\frac{dq}{dt} = \frac{\Delta I(r)}{L} = I_0(r)\frac{(1-e^{-\alpha_a L})}{L}. \quad (3)$$

This is equivalent to

$$\frac{dq}{dt} = I_0(r)\alpha_{eff} \quad (4)$$

Where, in order to use the same methods, equations and analysis already established in [36], one should introduce an effective absorption coefficient defined as:

$$\alpha_{eff} = \frac{(1-e^{-\alpha_a L})}{L}. \quad (5)$$

This definition of α_{eff} indicates that the actual heat absorbed by the suspension is smaller than what could be calculated considering a 1st order limited expansion. Moreover, note that the dimension of α_{eff} in m^{-1} should not be confused with $L_{eff} = (1 - e^{-\alpha_a L})/\alpha_a$ which is used in nonlinear optics when measuring the third order susceptibility coefficient (see for example [37]). Here, α_{eff} could replace the absorption in the derived equations of Sheldon et al. [36] to define the phase lag characteristic quantity:

$$\theta = \frac{PLdn/dT}{\lambda k}\alpha_a \qquad (6)$$

with dn/dT denoting the algebraic value of the thermo-optical coefficient. Then in our more general case, θ_{eff} is defined relative to α_{eff} and should be considered as:

$$\theta_{eff} = \frac{PLdn/dT}{\lambda k}\alpha_{eff} = \frac{Pdn/dT}{\lambda k}[1 - exp(-\alpha_a L)]. \qquad (7)$$

So, the variation in temperature in the medium, taking into account the aberrant nature of the TL [36, 38], is given by:

$$\Delta T(r,t) = \frac{2P\alpha_{eff}}{\pi c\rho\omega^2}\int_0^t \left(\frac{1}{1+2t'/t_c}\right) exp\left(\frac{-2r^2/\omega^2}{1+2t'/t_c}\right) dt', \qquad (8)$$

where $t_c = c\rho\omega^2/4k$ is the characteristic buildup time constant. The change in the linear index due to this temperature variation is:

$$\Delta n(r,t) = \frac{dn}{dT}\Delta T(r,t), \qquad (9)$$

with $\Delta n(r,t) = n(r,t) - n_0$ where n_0 is the refractive index at the initial temperature. The phase shift is related to Δn as usual, using $\Delta\varphi = 2\pi\Delta nL/\lambda$. The single-beam configuration that we consider here states that the beam induces $\Delta\varphi$ and probes it at the same time.

3. METHODS

a. Principle of the optical method

The TL schematic diagram of the method is shown in Fig. 1. This setup has the advantage

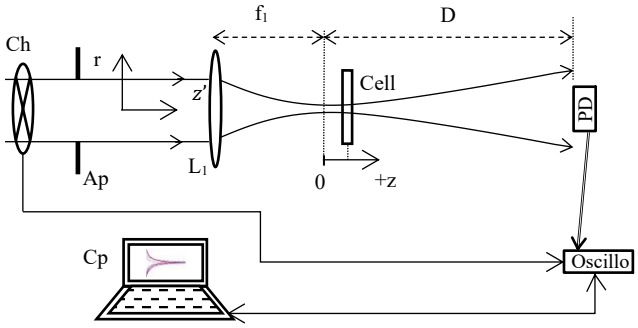

Fig. 1: Scheme showing the different position of the optical elements. The cell is scanned along the beam direction around the focal plane (z=0). The labels refer to: lens (L_1), chopper (Ch), circular aperture (Ap), computer (Cp) and photodiode (PD).

of combining a Z-scan configuration when the sample moves along z (focal region of lens L_1) and a TL signal describing the time response profile when the chopper rotates for each position z (for details see [35]). The signal due to the phase shift as a consequence of temperature change in the sample is obtained on a photodiode (PD) (Thorlabs, DET10A/M) that acquires the central variation of the diffracted far field beam intensity versus z, the position of the specimen. This is equivalent to performing what is commonly referred to as a "closed aperture Z-scan". The Si PD, 1 ns rise time, 0.8 mm^2 is connected to an oscilloscope (Agilent, DSOX3054A 500MHz). The signal is supposed to be only revealed by a thermal lens effect which allows the measurement of α_a. The cell is fixed on a motorized linear stage (Standa, 8MT295) permitting the sample to be scanned along z. The refractive signal (S) is defined as being the fractional intensity change when the cell is located at z after reaching the stationary regime (at $t \to \infty$):

$$S(z) = \frac{[I(z,t=0)-I(z,\infty)]}{I(z,\infty)}. \qquad (10)$$

The analytical calculations for the far field intensity variation provided in [36] at $r = 0$, gives:

$$S(V) = -1 + \frac{1}{1-\theta_{eff}tan^{-1}\left(\frac{2V}{3+V^2}\right)} \qquad (11)$$

where $V = z/Z_0$ with the Rayleigh distance $Z_0 = \pi\omega_{0f}^2/\lambda$ and ω_{0f} being the focused beam-waist at $z = 0$ (the focus of lens L_1). Eq. *(11)* allows to obtain θ_{eff} by fitting the experimental data normalized according to Eq. *(10)*. Following relationship (7), one can then find α_a, *i.e.,* the light truly absorbed in the medium:

$$\alpha_a = \frac{1}{L} ln \left[\frac{Pdn/dT}{Pdn/dT - \lambda k \theta_{eff}} \right]. \quad (12)$$

On the other hand, the average value of the extinction coefficient of the specimen α_e is measured precisely using an optical power meter (OPM) (Ophir, PD300UV, $10x10\,mm$ aperture) by repeating the measurement several times while varying the incident power: $\alpha_e = ln(P_0/P_C)/L$ with P_0 being the transmitted power by the pure solvent and P_C the transmitted one by the concentration of the nanoparticles that will be used in the experiment. The latter relation is used in order to take into account the Fresnel reflection with two identical cells. Note that the accuracy of this measurement has been greatly improved compared to [35]. Indeed, the measurement is made with an order of magnitude higher accuracy. By placing the sample at the entrance of the setup through the collimated beam, a larger illuminated area of the suspension under test is covered (2 mm diameter), whereas previously the sample was placed in the focal plane with a beam waist around $20\ \mu m$.

Let Φ represent the ratio between the number of scattered photons to that of extinguished ones. The scattering could account for fluorescence, luminescence or the light energy which has been spread out of propagation-axis by the nanoparticles depending on their size. This leads to the calculation of the light scattering efficiency Φ relative to the total light extinction with the following equation (see calculation details in annex A):

$$\Phi = \frac{exp(-\alpha_a L) - exp(-\alpha_e L)}{[1 - exp(-\alpha_e L)]}. \quad (13)$$

Note that $1 - \Phi = [1 - exp(-\alpha_a L)]/[1 - exp(-\alpha_e L)]$ represents the fraction of the light extinction that is not scattered but absorbed by the NPs leading to photothermal heating and to the observation of the TL signal. This term characterizes the photothermal efficiency.

b. Preparation of the suspensions

An aqueous solution of spherical gold NPs of 5 nm diameter (maximum of absorption $517\ nm$) was obtained from [39] and used as received, diluting with pure water when required. Colloidal gold nanospheres of 40, 60 and 80 nm diameter in water, stabilized by citric acid, were obtained from Sigma-Aldrich and further processed according to an established protocol.[40] An aqueous solution of 0.2 mM sodium lipoate (NaLA) and 1 mM NaOH was prepared using racemic (±)-α-lipoic acid (LA, Sigma, 0.2 mM) and NaOH (1.2 mM) in pure water. The colloidal gold NPs (40, 60, 80 nm diameter) were coated with lipoate by mixing them with the aqueous NaLA solution. Samples were centrifuged (Hettich Mikro 220R, Germany) for 30 min at a centrifuge speed adapted for each particle diameter.[41] After each centrifugation step, the supernatant was removed and replaced (90% of the volume) by fresh aqueous NaLA-NaOH solution. This centrifugation-redispersion was repeated two times and the particles were finally dispersed in a total volume of 1 mL aqueous solution (0.2 mM NaLA, 1 mM NaOH). The samples were characterized using optical extinction (UV-visible) spectroscopy comparing the spectra of the LA-functionalized gold gold NSs to the spectra of the as-received solutions. No significant changes were found in the extinction spectra, confirming the integrity of the NPs. Transmission electron microscopy images are shown in Fig. 2. Images a.1), a.2), a.3) and a.4) show groups of $80\ nm$, $60\ nm$, $40\ nm$ and $5\ nm$ nanoparticles respectively with absorption maxima (Fig. 2b) at $555\ nm$, $542\ nm$, $529\ nm$ and $516\ nm$, in line with the predictions from Mie theory.

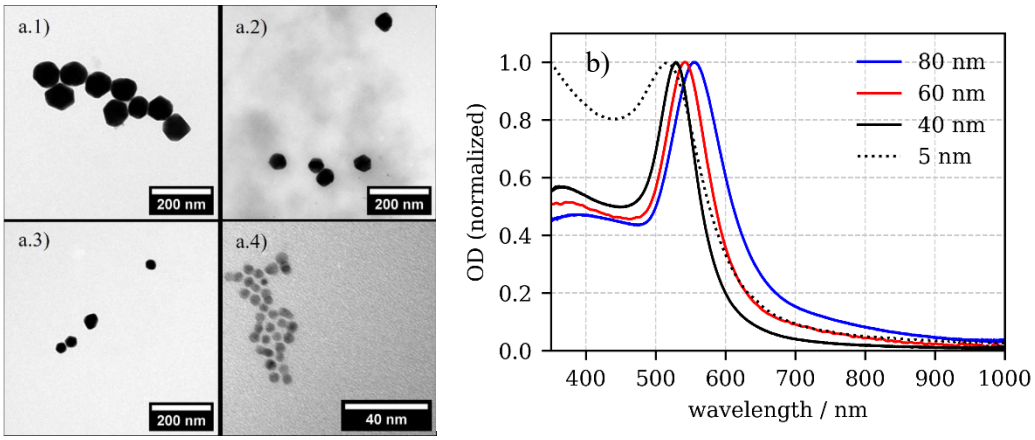

Fig. 2: TEM images of the gold nanospheres of diameter 80 nm (a.1), 60 nm (a.2), 40 nm (a.3) and 5 nm (a.4). (b) Normalized extinction spectra of the suspensions.

4. Experimental results

The study has been performed using three different wavelengths: 473 nm, 532 nm and 638 nm at the output of three different cw lasers (MSL-FN-473; LCX-532S; MDL-C-637). The lasers were aligned on the same optical axis of the setup shown in Fig. 1 and used separately one at a time. A new configuration of the experimental setup was implemented compared to the previous one [35] because of the poor optical quality of the spatial profiles of the Gaussian beams at the output of the new lasers (red and blue). Therefore, the output laser beams were spatially filtered before collimation and truncated by a circular aperture resulting in a "top-hat" beam of diameter $\approx 2\ mm$. They were then focused into the quartz cell (Thorlabs, CV10Q35) containing the NP suspensions. The rotation of the two-bladed chopper (Thorlabs, MC 1000) was set at a frequency of $10\ Hz$ which gives $50\ ms$ of opening time during which the solution is irradiated and $50\ ms$ of obstruction allowing the liquid to cool down between two acquisitions. These exposure times provide a sufficient duration for the temporal evolution to reach the nearly stationary regime. Typically, with $\omega_{0f} = 50.8\ \mu m$, the thermal response time of the water solvent is characterized by $t_c = c\rho\left(\omega_{0f}\right)^2/4k \approx 5\ ms$. This time can be regarded as very small when compared to the opening duration of the chopper.

a. Features of the measurement system

As an illustration, an experimental result is provided here using the 638 nm laser with an aqueous solution of 5 nm diameter gold NPs. The blue stars experimental data in Fig. 3a ($S(V)$) are normalized using *Eq. 10* and show a characteristic valley-peak profile. They are numerically processed to be symmetrical with respect to $V = 0$. Using *Eq. 11*, the fitting of $S(V)$ allows to estimate the Airy pattern in the focal plane equivalent to a Gaussian beam having a given beam-waist by adjusting the diameter of the circular aperture such that $Z_0 \geq L$. For instance, for the acquisition presented in Fig. 3, the diameter of the aperture was adjusted to 2 mm giving $\omega_{0f} = 50.8\ \mu m$. This value corresponds to a Rayleigh distance of $Z_0 = 1.27\ cm$ (using a focal lens $f_1 = 25\ cm$). The thickness of the cell ($L = 1\ cm$) is therefore compatible to be considered as a thin sample. Note that the incident power (inside the liquid) in this example was $P = 1.1\ mW$ resulting in a central peak intensity in the focus at $z = 0$, $I_0 = 0.28\ MW/m^2$. Using an open aperture Z-scan configuration (as previously done in [35], figure 1) it was experimentally confirmed that no nonlinear absorption could be measured, which makes sense since nonlinear effects could occur with much higher intensities ($at \sim 0.1 GW/cm^2$) which is 6 orders of magnitude higher.

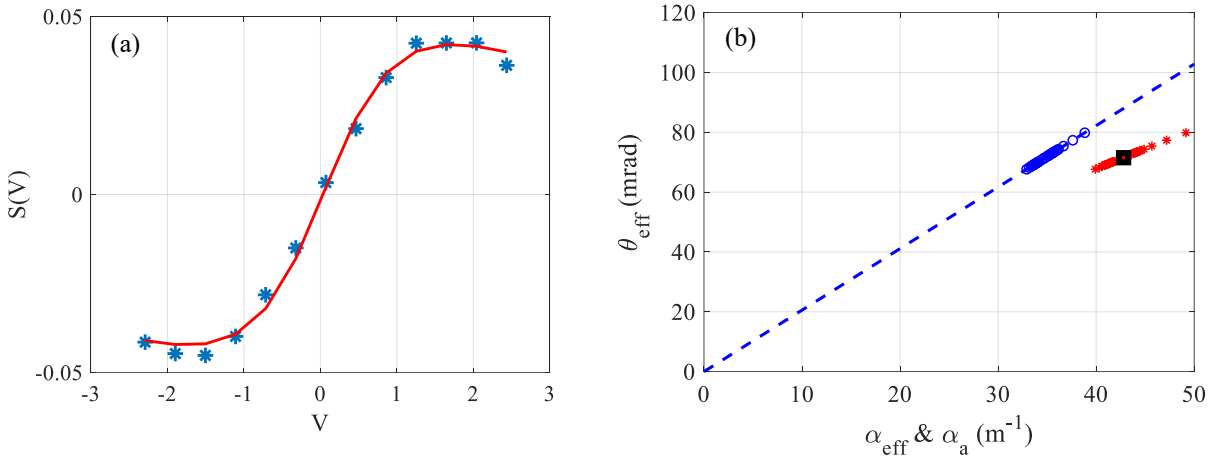

Fig. 3: Gold NPs of 5nm in water (a) Fitting (red solid line) of the Z-scan profile (blue stars) versus the normalized position V allowing to obtain θ_{eff}. (b) Results of the fitting over 52 acquisitions giving θ_{eff} as a function of α_{eff} (blue circle) and α_a (red stars). The black square gives the mean value.

The solid red line in Fig. 3(a) shows the fitting of the experimental data (blue stars) giving $\theta_{eff} = 80.5\, mrad$ with a solution having an overall attenuation coefficient $\alpha_e = 42.8 \pm 0.4\, m^{-1}$ measured in a standard light transmission experiment via the OPM. Following *Eq. (7)*, one can obtain the value of $\alpha_{eff} = 34.63\, m^{-1}$ knowing $L = 1\, cm$, $\lambda = 638\, nm$, $dn/dT = -0.8 \times 10^{-4} K^{-1}$ and $k = 0.61\, J/s/m/K$ for water. The value of the absorption can be obtained from *Eq. (12)* giving $\alpha_a = 42.5\, m^{-1}$. This single measurement value is slightly different from the value found by the direct transmission measurement. To obtain a higher accuracy, it was necessary to repeat the same procedure several times. This is shown in Fig. 3(b) where we have performed 52 Z-scan profiles in the same experimental conditions to obtain an average value of $\alpha_a = 42.8 \pm 1.8\, m^{-1}$ (represented by a black square). The absolute error is calculated by taking into account the standard deviation σ over the 52 observations. It is thus found experimentally that $\alpha_a \approx \alpha_e$ for these 5 nm gold NPs, i.e., the overall extinction is dominated by thermally dissipated photoabsorption, and light scattering by these NPs is negligible. This agrees with Mie theory for $5\, nm$ spherical gold NP which predicts a negligible scattering efficiency ($< 10^{-3}$) at $638\, nm$ corresponding to a photothermal absorption efficiency of 1. Note that in Fig. 3(b) one can see obviously that the values of α_a and α_{eff} are not equal even with relatively moderate absorbance: $\alpha_a L \approx 0.4 < 1$. This proves the benefit of introducing α_{eff} defined in *Eq. (5).*

Moreover, to check that the theoretical calculations using the effective absorption are relevant, we also studied the influence of the concentration on the measurement of α_a. For this purpose, Fig. 4 represents the results of the experiment carried out on 4 different concentrations of 80 nm gold NP, i.e., different extinction coefficients ($\alpha_e = 22.6\, m^{-1}, \alpha_e = 50.2\, m^{-1}, \alpha_e = 64.6\, m^{-1}, \alpha_e = 90.1\, m^{-1}$) and with different incident laser powers ($0.92\, mW < P < 2.72\, mW$) at $\lambda = 532\, nm$. Using *Eq. (13),* it is possible to extract α_a as a function of α_e: $\alpha_a = -ln\{\Phi[1 - exp(-\alpha_e L)] + exp(-\alpha_e L)\}/L$. The plot of the variation (solid red line) using the

experimental value obtained for light scattering efficiency $\Phi = 0.35$ (see Table 1) shows a very good agreement with the experimental data for the 4 groups of concentrations relative to the 4 labeled α_e inside Fig. 4. The dashed black line corresponds to the calculation using the usual

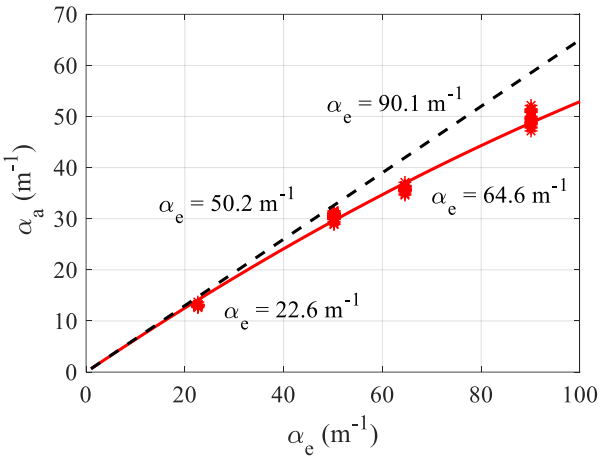

Fig. 4: α_a versus α_e (red stars) at $\lambda = 532$ nm for 80 nm NP with different absorbances: $0.2 < \alpha_e L < 0.9$. The solid red line is given by Eq. 13 for the experimental measured value $\Phi = 0.35$. The dashed black line shows the variation of the same parameters using A4 considering the usual approximations.

first-order approximation for low absorption (Eq. A4) considering the same light scattering efficiency of 0.35. The difference between the two curves gets larger with the concentration which would induce higher errors of the measurement for relatively higher absorbing concentrations. Note the occurring of an error as large as 20% with $\alpha_e L = 0.9$ when evaluating α_a.

The linearity of the response at $\theta_{eff} > 106\ mrad$ was tested. It has been mentioned [35, 36] that a nonlinearity appears beyond this value. Fig. 5 shows the experimental results at $\lambda = 532\ nm$ done on $5\ nm$ NPs at a concentration having $\alpha_e = 91.1\ m^{-1}$ with $L = 1\ cm$. The measured θ_{eff} is shown as a function of the incident power P. It can be clearly seen that the response remains linear even at θ_{eff} values higher than $106\ mrad$. This was made possible by the introduction of α_{eff}. Despite the large dynamics of the system response, it should be noted that all the results presented in this paper are determined with θ_{eff} values lower than

150 $mrad$. In other words, we optimized the acquisitions to obtain a large signal with low incident power.

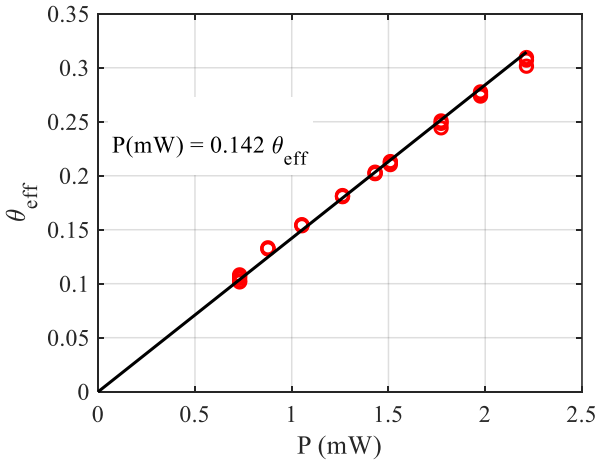

Fig. 5: θ_{eff} versus P for a 5 nm NP sample with $\alpha_e = 91.1\ m^{-1}$. The solid black line is the linear fitting having a slope of $0.142\ mW^{-1}$.

The black solid line (Fig. 5) represents the linear fit of the experimental points by forcing the least mean squares line through zero. The slope of this line is equal to $0.142 \pm 0.01\ mW^{-1}$ when it should theoretically be equal to:

$$\frac{\theta_{eff}}{P_e} = \frac{L\alpha_{eff}dn/dT}{\lambda k} = \frac{10^{-2}\times 59.78\times 8\times 10^{-5}}{532\times 10^{-9}\times 0.61} = 0.147\ \mathrm{mW}^{-1}. \qquad (14)$$

The value found by the linear fitting is in good agreement with the supposed theoretical value based on the literature for dn/dT which shows the reliability and the accuracy of the developed method.

b. Mie theory versus experiments

Theoretical values of the optical cross sections (extinction, scattering, absorption) and derived quantities for spherical gold nanoparticles in water ($n = 1.33$) were obtained by numerically evaluating the analytic expressions from Mie theory.[42] The evaluation was done using a published Python program[43] (with the numpy[44] and scipy[45] numerical scientific libraries) based on MATLAB code by Mätzler.[46] The dielectric function for gold used in the

calculations was obtained by interpolation of the experimental optical constants by Johnson & Cristy.[47] A correction to this bulk dielectric function to account for the reduced mean-free path (MFP) of the conduction electrons in small particles was applied.[48] Application of this MFP correction lead to significantly better agreement with the experimental data compared to the uncorrected bulk dielectric function.

Using the measurement method described and validated above, we studied the photothermal efficiency for spherical gold nanoparticles of varying diameter in water as a function of laser wavelength (437 nm, 532 nm, and 638 nm). The photothermal efficiency of each gold NP diameter was measured following *Eq. (13)* and is plotted as a function of the laser wavelength. Theoretical values were obtained from the absorption (σ_{abs}) and extinction (σ_{ext}) cross sections calculated using Mie theory, applying $(1-\Phi) = \sigma_{abs}/\sigma_{ext}$.

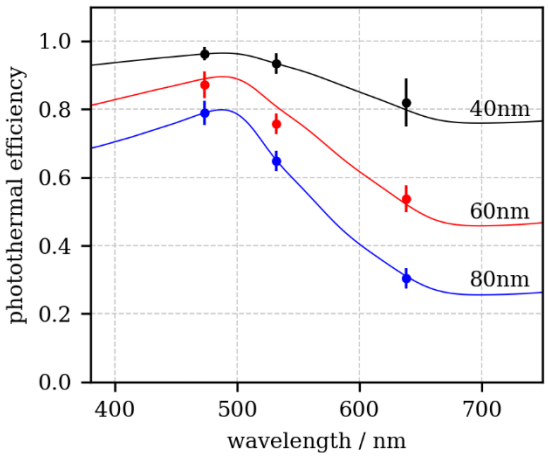

Fig. 6: The photothermal efficiency $(1-\Phi)$ as a function of wavelength for 40, 60 and 80 nm spherical gold NPs in water. The points with the error bars are the experimental values obtained by TLS. The solid lines are the wavelength-dependent photothermal efficiencies calculated using Mie theory. The dielectric function for gold was corrected for the electrons' mean free path.

All results are summarized in the form of Fig. 6. The simulated photothermal efficiency spectra with Mie theory are shown by the solid lines: the blue one is relative to the 80 nm NPs, the red one to the 60 nm and the black one to the 40 nm. The experimental results are represented by dots with their error bars (for details of error calculations see appendix A). They are in good

agreement with the theory, all measurements except one ($60\ nm$ NP at $532\ nm$) have their simulated value inside the error bar. This demonstrates the relevance of the present TL experiment, allowing to precisely measure the photothermal light absorption of the samples, which can be used to infer the scattering efficiency in the case of plasmonic NPs. Table 1 shows the data of Fig. 6 with additional information such as the extinction and absorption coefficients measured at each case.

NP	$\lambda = 638\ nm$				$\lambda = 532\ nm$			
	$\alpha_e(m^{-1})$	$\alpha_a(m^{-1})$	$(\Phi \pm \Delta\Phi)(\%)$	$\Phi_t(\%)$	$\alpha_e(m^{-1})$	$\alpha_a(m^{-1})$	$(\Phi \pm \Delta\Phi)(\%)$	$\Phi_t(\%)$
5 *nm*	42.8	42.7	0.1±4	0.07	59.9	59.7	0.3±4	0.01
40 *nm*	31.6	25.2	18.0±7	26.5	73.0	66.3	6.5±3	7.2
60 *nm*	33.2	16.5	46.3±4	53.3	71.8	49.2	24.2±3	19.1
80 *nm*	76.5	17.9	69.5±3	72.6	58.3	33.4	35.1±3	36.2

$\lambda = 473\ nm$				
NP	$\alpha_e(m^{-1})$	$\alpha_a(m^{-1})$	$(\Phi \pm \Delta\Phi)(\%)$	$\Phi_t(\%)$
5 *nm*	50.23	50.17	0.08 ± 4.7	0.8
40 *nm*	107.4	100.4	3.7 ± 2	3.75
60 *nm*	87.6	71.1	12.8 ± 4	11.3
80 *nm*	106.8	77.5	21.0 ± 3.6	21.4

Table 1 : Experimental values of Φ, the scattering efficiency relative to the nanoparticles at 473 nm, 532 nm and 638 nm. Φ_t is the theoretical value.

From Fig. 6, it is seen that there is a marked wavelength-dependence of the photothermal absorption efficiency, meaning that the fraction of light in the extinction by the NP solution leading to heating varies with wavelength. For these spherical gold nanoparticles, the photothermal efficiency is higher at shorter wavelengths and decreases towards longer wavelengths. It is at these longer wavelengths that the scattering process becomes more efficient. In addition, there is a relationship between the size of the particles in the suspensions,

the incident wavelength and its ability to convert light into thermal energy. The size of the nanostructures is an important parameter in determining its photothermal efficiency. Smaller particles have a larger surface area to volume ratio, which increases their absorption of light relative to scattering and hence their conversion into heat. Therefore, it is reasonable to expect that as the diameter of a structure decreases, its photothermal efficiency would increase. It is a useful general guideline; a more detailed analysis is needed to fully understand the relationship between these parameters and a material's ability to convert light into heat energy especially in the case of nanorods.

c. Discussion

It is important to note that for evaluating the overall photothermal heating by NPs, the extinction cross section and the NP concentration should be taken into account. The interest of considering here the photothermal efficiency $(1 - \Phi)$ is that it can be measured without knowing the particle concentration and the extinction cross section, while the experimental results still can be compared to the theoretical calculations. This is useful for the characterization of novel (non-spherical) NPs and NP assemblies whose optical properties cannot easily be calculated from theory. It is also useful for validating new theoretical and numerical models for calculating the optical properties of such NPs and NP assemblies. Moreover, our experimental and simulation results of Table 1 shown in Fig. 6 are in a very good agreement with the theoretical results obtained by Jain et al. in [1] where they perform a simulation to determine the absorption and extinction coefficients of spherical gold NP with different diameters and shapes according to an improved Mie Theory. Let's not forget that the theoretical curves are for ideal samples, perfectly spherical particles with diameter exactly equal to 5, 40, 60 or 80 nm. Real samples do not correspond exactly to this ideal, and deviations between theory and experiment are therefore possible.

Measuring absorption and scattering efficiencies has been shown here under different experimental parameters and conditions. The understanding of nanoparticles scattering, and quantum yields measurements are crucial for photothermal applications, especially for the medical area where the majority of imaging and therapeutic techniques are subject to this phenomenon. At the dimensional metrology level, this may also be an adequate solution for certain types of problems where a doping in nanoparticles would improve the contrast and facilitate the measurements [49]. The photothermal lens technique presented here allows an accurate measurement of the fraction of excitation energy that does not leave the nanoparticle system as scattered light but is absorbed and converted into photothermal heat. Furthermore, the technique may also be applied to the characterization of molecular phosphorescence and fluorescence in solution. It is believed that this photothermal lens measurement is among the most accurate means of measuring photothermal conversion because the sample disturbance and stress are minimal. Only one milliwatts of excitation light pass through the sample and the temperature rise is negligible ($< 10^{-1} °C$). [32] The excitation is modulated ($50\ ms$ "on", $50\ ms$ "off"), which allows the sample to cool down and return to equilibrium after each cycle. All this allows to stay in a linear response regime and to avoid a number of possible complications and artifacts. In addition, the Z-scan photothermal lens technique allows an absolute measurement without the need for reference samples. An interesting perspective would be to enlarge the range of excitation wavelengths to go towards a true photothermal spectroscopy.

5. Conclusions

The objective of this study was to determine the main characteristics of a measurement method easy to tune from one wavelength to another using circular top-hat beams inside a technique combining Z-scan with thermal lens methods. The measurements on spherical gold NPs in solution show that the photothermal efficiency fully explains the effective fraction of light power absorbed by the sample. The characteristics of the response was checked varying

either the incident power or the concentration. The relationship between the slope of this response and the thermo-optical characteristics of the absorbing liquid was determined precisely. The results were applied to the determination of the photothermal efficiency on gold spherical nanoparticles of 5, 40, 60 and $80\ nm$ diameters in the blue, the green and the red wavelengths. Then, we focused on the determination of the measurement error from statistical calculations. Our results show good agreement between the experimentally measured photothermal efficiencies and those calculated with Mie theory.

Appendix

Here, we derive the analytical calculation of the quantum yield Φ relative to the ratio between to the number of scattered photons N_s to that extinguished N_e. Let N be the total number of the incident photons and N_t the number of the transmitted ones, in the case where there is only absorption: $N = N_a + N_t$. The Beer–Lambert law states $N_t/N = exp(-\alpha_a L)$, giving then:

$$\frac{N_a}{N} = 1 - exp(-\alpha_a L). \qquad (A1)$$

Assuming now that part of the photons that we do not detect at the OPM is scattered (N_s) , the number of the extinguished photons writes: $N_e = N_a + N_s$ with $N = N_e + N_t$. The same Beer–Lambert law gives: $N_t/N = (N - N_e)/N = 1 - N_e/N = exp(-\alpha_e L)$ which gives:

$$\frac{N_e}{N} = 1 - exp(-\alpha_e L). \qquad (A2)$$

If we define the scattering efficiency by the ratio: $\Phi = \frac{N_s}{N_e} = \frac{N_e - N_a}{N_e}$ and taking into account *Eqs. (A1) and (A2)*, one can writes:

$$\boldsymbol{\Phi} = \frac{exp(-\alpha_a L) - exp(-\alpha_e L)}{[1 - exp(-\alpha_e L)]}. \qquad (A3)$$

In the case of small absorptions, $\alpha_a L \ll 1$ and $\alpha_e L \ll 1$, then we find the relation used in [35] with $L = 1\ mm$.

$$\boldsymbol{\Phi} \approx \frac{1 - \alpha_a L - (1 - \alpha_e L)}{\alpha_e L} = 1 - \frac{\alpha_a}{\alpha_e}. \qquad (A4)$$

It is easy to calculate the relative error obtained on Φ when we have an estimation of the absolute errors on α_e and α_a, $\Delta\alpha_e$ et $\Delta\alpha_a$, respectively. Theoretically:

$$\Delta\Phi = \frac{\partial\Phi}{\partial\alpha_e}\Delta\alpha_e + \frac{\partial\Phi}{\partial\alpha_a}\Delta\alpha_a,$$

By deriving relation *(A3)*, we get:

$$\frac{\Delta\Phi}{\Phi} = \frac{L}{(exp(-\alpha_a L) - exp(-\alpha_e L))}\left[\frac{(1-exp(-\alpha_e L))}{(1-exp(-\alpha_a L))} exp(-\alpha_e L)\Delta\alpha_e + exp(-\alpha_a L)\Delta\alpha_a\right] \quad (A5)$$

As an example, let us consider the $40\ nm$ NPs in the red with: $\alpha_e = 31.6\ m^{-1} \pm 1\%$, $\alpha_a = 25.2\ m^{-1} \pm 8\ \%$ and $L = 1\ cm$. The absorption relative errors are given by the standard deviation from statistics of experimental results obtained over a large number of acquisitions. We find $\Phi = 0.18$ and $\frac{\Delta\Phi}{\Phi} = 38\ \%$. Fig. A1 shows the evolution of $\frac{\Delta\Phi}{\Phi}$ versus α_e varying around the experimental measured value between $10\ m^{-1}$ and $100\ m^{-1}$. Note that the error decreases with increasing α_e hence the importance of considering relatively high value of absorption. Moreover, the lower the scattering efficiency, the larger the value of α_e to consider. The same analysis applies for the measurement of the absorption efficiency with a high scattering solution. Once again, the relative error can be minimized by increasing the extinction α_e for instance by increasing its concentration.

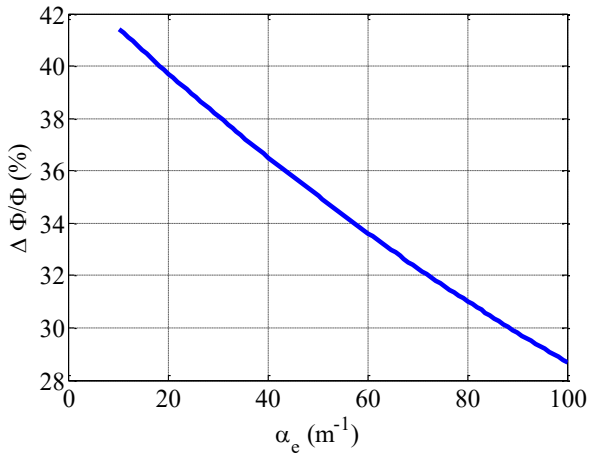

Fig. A1: Evolution of the relative error versus the overall absorption α_e in the case of $\Phi = 0.18$, with $\frac{\Delta\alpha_e}{\alpha_e} = 1\%$ and $\frac{\Delta\alpha_a}{\alpha_a} = 8\%$.

REFERENCES

[1] Jain, P. K., Lee, K. S., El-Sayed, I. H., & El-Sayed, M. A. (2006). Calculated absorption and scattering properties of gold nanoparticles of different size, shape, and composition: applications in biological imaging and biomedicine. The journal of physical chemistry B, 110(14), 7238-7248.
https://doi.org/10.1021/jp057170o

[2] Navarro, J. R., & Werts, M. H. (2013). Resonant light scattering spectroscopy of gold, silver and gold–silver alloy nanoparticles and optical detection in microfluidic channels. Analyst, 138(2), 583-592.
https://doi.org/10.1039/c2an36135c

[3] Baffou, G., Quidant, R., & García de Abajo, F. J. (2010). Nanoscale control of optical heating in complex plasmonic systems. ACS nano, 4(2), 709-716.
https://doi.org/10.1021/nn901144d

[4] Yelin, D., Oron, D., Thiberge, S., Moses, E., & Silberberg, Y. (2003). Multiphoton plasmon-resonance microscopy. Optics express, 11(12), 1385-1391.
https://doi.org/10.1364/OE.11.001385

[5] Chen, J., Wiley, B., Li, Z. Y., Campbell, D., Saeki, F., Cang, H., ... & Xia, Y. (2005). Gold nanocages: engineering their structure for biomedical applications. Advanced materials, 17(18), 2255-2261.
https://doi.org/10.1002/adma.200500833

[6] Ishii, S., Sugavaneshwar, R. P., & Nagao, T. (2016). Titanium nitride nanoparticles as plasmonic solar heat transducers. The Journal of Physical Chemistry C, 120(4), 2343-2348.
https://doi.org/10.1021/acs.jpcc.5b09604.

[7] Fairbairn, N., Christofidou, A., Kanaras, A. G., Newman, T. A., & Muskens, O. L. (2013). Hyperspectral darkfield microscopy of single hollow gold nanoparticles for biomedical applications. Physical Chemistry Chemical Physics, 15(12), 4163-4168.
https://doi.org/10.1039/C2CP43162A

[8] Yguerabide, J., & Yguerabide, E. E. (2001). Resonance light scattering particles as ultrasensitive labels for detection of analytes in a wide range of applications. Journal of Cellular Biochemistry, 84(S37), 71-81.
https://doi.org/10.1002/jcb.10077

[9] Derkowska-Zielinska, B., Barwiolek, M., Cassagne, C., & Boudebs, G. (2020). Nonlinear optical study of Schiff bases using Z-scan technique. Optics & Laser Technology, 124, 105968.
https://doi.org/10.1016/j.optlastec.2019.105968

[10] de Araújo, C. B., Falcão-Filho, E. L., Humeau, A., Guichaoua, D., Boudebs, G., & Kassab, L. R. (2005). Picosecond third-order nonlinearity of lead-oxide glasses in the infrared. Applied Physics Letters, 87(22), 221904.
https://doi.org/10.1063/1.2137457

[11] Fedus, K., Boudebs, G., Coulombier, Q., Troles, J., & Zhang, X. H. (2010). Nonlinear characterization of GeS 2–Sb 2 S 3–CsI glass system. Journal of Applied Physics, 107(2), 023108.
https://doi.org/10.1063/1.3289607

[12] Manzani, D., De Araújo, C. B., Boudebs, G., Messaddeq, Y., & Ribeiro, S. J. (2013). The role of Bi2O3 on the thermal, structural, and optical properties of tungsten-phosphate glasses. The Journal of Physical Chemistry B, 117(1), 408-414.
https://doi.org/10.1021/jp3097296

[13] Loumaigne, M., Vasanthakumar, P., Lombardi, A., Richard, A., & Débarre, A. (2013). One-photon excited luminescence of single gold particles diffusing in solution under pulsed illumination. *Physical Chemistry Chemical Physics*, *15*(12), 4154-4162.
https://doi.org/10.1039/C2CP43294C

[14] Shortell, M. P., Hewins, R. A., Fernando, J. F., Walden, S. L., Waclawik, E. R., & Jaatinen, E. A. (2016). Multi-angle fluorometer technique for the determination of absorption and scattering coefficients of subwavelength nanoparticles. Optics Express, 24(15), 17090-17102.
https://doi.org/10.1364/OE.24.017090

[15] Loumaigne, M., Navarro, J. R., Parola, S., Werts, M. H., & Débarre, A. (2015). The intrinsic luminescence of individual plasmonic nanostructures in aqueous suspension by photon time-of-flight spectroscopy. Nanoscale, 7(19), 9013-9024.
https://doi.org/10.1039/C5NR00363F

[16] Loumaigne, M., Midelet, C., Doussineau, T., Dugourd, P., Antoine, R., Stamboul, M., ... & Werts, M. H. (2016). Optical extinction and scattering cross sections of plasmonic nanoparticle dimers in aqueous suspension. Nanoscale, 8(12), 6555-6570.

https://doi.org/10.1039/c6nr00918b

[17] Midelet, J., El-Sagheer, A. H., Brown, T., Kanaras, A. G., Débarre, A., & Werts, M. H. (2018). Spectroscopic and Hydrodynamic Characterisation of DNA-Linked Gold Nanoparticle Dimers in Solution using Two-Photon Photoluminescence. ChemPhysChem, 19(7), 827-836.

https://doi.org/10.1002/cphc.201701228

[18] Richardson, H. H., Carlson, M. T., Tandler, P. J., Hernandez, P., & Govorov, A. O. (2009). Experimental and theoretical studies of light-to-heat conversion and collective heating effects in metal nanoparticle solutions. Nano letters, 9(3), 1139-1146.

https://doi.org/10.1021/nl8036905.Experimental

[19] Jiang, K., Smith, D. A., & Pinchuk, A. (2013). Size-dependent photothermal conversion efficiencies of plasmonically heated gold nanoparticles. The Journal of Physical Chemistry C, 117(51), 27073-27080.

https://doi.org/10.1021/jp409067h

[20] Ciancone, M., Bellec, N., & Camerel, F. (2020). IPT: An Index to Rank Molecular Photothermal Agents. ChemPhotoChem, 4(12), 5341-5345.

https://doi.org/10.1002/cptc.202000088

[21] Whinnery, J. R. (1974). Laser measurement of optical absorption in liquids. Accounts of Chemical Research, 7(7), 225-231.

https://doi.org/10.1021/ar50079a003

[22] Carter, C. A., & Harris, J. M. (1984). Comparison of models describing the thermal lens effect. Applied Optics, 23(3), 476-481.

https://doi.org/10.1364/AO.23.000476

[23] Snook, R. D., & Lowe, R. D. (1995). Thermal lens spectrometry. A review. Analyst, 120(8), 2051-2068.

https://doi.org/10.1039/an9952002051

[24] Tokeshi, M., Uchida, M., Hibara, A., Sawada, T., & Kitamori, T. (2001). Determination of subyoctomole amounts of nonfluorescent molecules using a thermal lens microscope: subsingle-molecule determination. Analytical chemistry, 73(9), 2112-2116.

https://doi.org/10.1021/ac001479g

[25] Cabrera, H., Akbar, J., Korte, D., Ramírez-Miquet, E. E., Marín, E., Niemela, J., ... & Franko, M. (2018). Trace detection and photothermal spectral characterization by a tuneable thermal lens spectrometer with white-light excitation. Talanta, 183, 158-163.
https://doi.org/10.1016/j.talanta.2018.02.073

[26] Jiménez Pérez, J. L., Gutierrez Fuentes, R., Sanchez Ramirez, J. F., & Cruz-Orea, A. (2008). Study of gold nanoparticles effect on thermal diffusivity of nanofluids based on various solvents by using thermal lens spectroscopy. The European Physical Journal Special Topics, 153(1), 159-161.
https://doi.org/10.1140/epjst/e2008-00417-5

[27] Shahriari, E., Yunus, W. M., & Zamiri, R. (2013). The effect of nanoparticle size on thermal diffusivity of gold nano-fluid measured using thermal lens technique. Journal of the European Optical Society-Rapid publications, 8.
https://doi.org/10.2971/jeos.2013.13026

[28] Sindhu Swapna, M. N., Raj, V., Cabrera, H., & Sankararaman, S. I. (2021). Thermal lensing of multi-walled carbon nanotube solutions as heat transfer nanofluids. ACS Applied Nano Materials, 4(4), 3416-3425.
https://doi.org/10.1021/acsanm.0c03219

[29] Marcano, A., Alvarado, S., Meng, J., Caballero, D., Moares, E. M., & Edziah, R. (2014). White light photothermal lens spectrophotometer for the determination of absorption in scattering samples. Applied Spectroscopy, 68(6), 680-685.
https://doi.org/10.1366/13-07385

[30] Hlaing, M., Gebear-Eigzabher, B., Roa, A., Marcano, A., Radu, D., & Lai, C. Y. (2016). Absorption and scattering cross-section extinction values of silver nanoparticles. Optical Materials, 58, 439-444.
https://doi.org/10.1016/j.optmat.2016.06.013

[31] Olaizola, A. M. (2018). Photothermal determination of absorption and scattering spectra of silver nanoparticles. Applied spectroscopy, 72(2), 234-240.
https://doi.org/10.1177/0003702817738056

[32] Pedrosa, T. L., Estupiñán-López, C., & De Araujo, R. E. (2020). Temperature evaluation of colloidal nanoparticles by the thermal lens technique. Optics Express, 28(21), 31457-31467.
https://doi.org/10.1364/OE.405172

[33] Zanuto, V. S., dos Santos, J. F. M., Baesso, M. L., & Catunda, T. (2021). Single-beam time-resolved cw thermal Z-scan analysis applied in solids. Optics & Laser Technology, 142, 107248.
https://doi.org/10.1016/j.optlastec.2021.107248

[34] Boudebs, G. (2021). Numerical simulation of the whole thermal lensing process with Z-scan-based methods using Gaussian beams. Materials, 14(19), 5533.
https://doi.org/10.3390/ma14195533

[35] Cassagne, C., Ba, O., & Boudebs, G. (2022). Time-Resolved cw Thermal Z-scan for Nanoparticles Scattering Evaluation in Liquid Suspension. Materials, 15(14), 5008.
https://doi.org/10.3390/ma15145008

[36] Sheldon, S. J., Knight, L. V., & Thorne, J. M. (1982). Laser-induced thermal lens effect: a new theoretical model. Applied optics, 21(9), 1663-1669.
https://doi.org/10.1364/AO.21.001663

[37] Besse, V., Boudebs, G., & Leblond, H. (2014). Determination of the third-and fifth-order optical nonlinearities: the general case. Applied Physics B, 116(4), 911-917.
http://dx.doi.org/10.1007/s00340-014-5777-2

[38] Carter, C. A., & Harris, J. M. (1984). Comparison of models describing the thermal lens effect. Applied Optics, 23(3), 476-481.
https://doi.org/10.1364/AO.23.000476

[39] https://www.sigmaaldrich.com/FR/fr/product/aldrich/752568

[40] Midelet, C., & Werts, M. H. (2020). Dielectrophoretically Modulated Optical Spectroscopy of Colloidal Nanoparticle Solutions in Microfluidic Channels. *Particle & Particle Systems Characterization*, *37*(10), 2000187.
https://doi.org/10.1002/ppsc.202000187.

[41] Midelet, J., El-Sagheer, A. H., Brown, T., Kanaras, A. G., & Werts, M. H. (2017). The sedimentation of colloidal nanoparticles in solution and its study using quantitative digital photography. *Particle & Particle Systems Characterization*, *34*(10), 1700095.
https://doi.org/10.1002/ppsc.201700095.

[42] Bohren, C. F., & Huffman, D. R. (1983). Absorption and Scattering of Light by Small Particles. Wiley-Interscience, New York.
https://doi.org/10.1017/S0263574798270858.

[43] Navarro, J. R., & Werts, M. H. (2013). Resonant light scattering spectroscopy of gold, silver and gold–silver alloy nanoparticles and optical detection in microfluidic channels. Analyst, 138(2), 583-592.
https://doi.org/10.1039/c2an36135c.

[44] Harris, C. R., Millman, K. J., Van Der Walt, S. J., Gommers, R., Virtanen, P., Cournapeau, D., ... & Oliphant, T. E. (2020). Array programming with NumPy. Nature, 585(7825), 357-362.
https://doi.org/10.1038/s41586-020-2649-2

[45] Virtanen, P., Gommers, R., Oliphant, T. E., Haberland, M., Reddy, T., Cournapeau, D., ... & Van Mulbregt, P. (2020). SciPy 1.0: fundamental algorithms for scientific computing in Python. Nature methods, 17(3), 261-272.
https://doi.org/10.1038/s41592-019-0686-2

[46] Mätzler, Christian. "MATLAB Functions for Mie Scattering and Absorption Version 2," 2002.
https://www.semanticscholar.org/paper/MATLAB-Functions-for-Mie-Scattering-and-Absorption-M%C3%A4tzler/86358e6a8504ff649818d17d10143cbcac18d28d

[47] Johnson, P. B., & Christy, R. W. (1972). Optical constants of the noble metals. Physical review B, 6(12), 4370.
https://doi.org/10.1103/PhysRevB.6.4370.

[48] Haiss, W., Thanh, N. T., Aveyard, J., & Fernig, D. G. (2007). Determination of size and concentration of gold nanoparticles from UV− Vis spectra. Analytical chemistry, 79(11), 4215-4221.
https://doi.org/10.1021/ac0702084.

[49] Boudebs, G., Chis, M., & Monteil, A. (1998). Contrast increasing by third-order nonlinear image processing: a numerical study for microscopic rectangular objects. Optics communications, 150(1-6), 287-296.
https://doi.org/10.1016/S0030-4018(98)00037-6